Desalination and Water Treatment
www.deswater.com
doi: 10.5004/dwt.2023.29569

294 (2023) 149–161
May

Separation of chromium(VI) by adsorption onto garlic peels: kinetics, thermodynamic and isotherm study

Z.M. Saigl*, E.E. Aloufi

Department of Chemistry, Faculty of Science, King Abdulaziz University, P.O. Box 80203, Jeddah 21589, Saudi Arabia, Tel.: +966-12-6952000 Ext: 26546; Fax: +966-12-6952292; email: zsaigl@kau.edu.sa/zeinabsaigl@hotmail.com (Z.M. Saigl), ealoufi0012@stu.kau.edu.sa (E.E. Aloufi)

Received 2 December 2022; Accepted 15 April 2023

ABSTRACT

Garlic peel, an agriculture by-product, was modified using nitric acid as a simple method. Therefore, this study aims to remove and/or minimize of Cr(VI) ions from aqueous media using HNO_3 modified garlic peel (HNO_3-GP). Scanning electron microscopy, energy-dispersive X-ray spectroscopy and Fourier-transform infrared spectroscopy analysis of the HNO_3-GP, as a solid phase extractor, were performed. The operational parameters of the adsorption such as solution pH, initial concentration of analyte, adsorbent dose, temperature and shaking time were performed. The equilibrium data of Cr(VI) showed a better fit with Langmuir isotherm model with R^2 = 0.9956 and adsorption capacity equals to 31.7 mg/g. Moreover, the kinetic data of analyte retained revealed that the present system fitted well with pseudo-second-order kinetic model (R^2 = 0.9918). Thermodynamic studies indicated that the retention step was endothermic and spontaneous in nature depending on the value of $\Delta H°$ (118.292 J/mol) and $\Delta G°$ (–117.41 kJ/mol). The positive value of $\Delta S°$ (394.39 J/mol·K) confirmed that the biosorption process was carried out with high randomness on the surface of HNO_3-GP. The results showed that the proposed adsorbent (HNO_3-GP) provides an effective and economical approach in highly minimization or almost removal of Cr(VI) ions from the aqueous solution.

Keywords: Chromium(VI); Garlic; Pseudo-second-order; Thermodynamic; Isotherm; Water samples

1. Introduction

Chromium is one of the heavy metals that have an oxidation states from +2 until +6 [1]. Due to its toxicity, Cr(VI) has received a great attention [2]. The use of chromium has increased right now due to the increase of industries which consequently rises its existence in the aqueous medium [3]. Cr(VI) has been used in several industries such as leather tanning, steel fabrication, metal finishing, electroplating [2] pigments, paints [3] plastic and textile industries [2,3]. Cr(VI) is considered to be more toxic than Cr(III) because its high-water solubility and mobility [4]. For this reason, it was classified as causing cancer to humanity [5]. People are exposed to chromium by ingestion through a food pipe or other paths such as inhalation and skin contact and then pile up in human tissues causing harmful diseases [3]. The maximum allowable limit of Cr(VI) is 0.1 mg/L for the drainage into inland surface water and 0.05 mg/L into drinkable water [3].

There are several instruments used to estimate Cr(VI) such as flame atomic absorption spectrometry (FAAS), graphite furnace atomic absorption spectrometry (GFAAS), UV-visible spectrophotometer, inductively coupled plasma mass spectrometry (ICP-MS) and inductively coupled plasma optical emission (ICP-OES) [6–10].

Several methods have been advanced to purify water from Cr(VI) including preconcentration and separation

* Corresponding author.

methods such as dispersive liquid–liquid microextraction (DLLME), single-drop microextraction (SDME), nanofiltration, electro membrane extraction (EME), liquid ion-exchange with cloud point extraction [7,9,11–13]. Each technique has many advantages and disadvantages [14,15]. For example, chemical precipitation method has the advantage of simple operation and low-cost, while one of its disadvantages is that great amounts of chemical products are created and thus lead to problems in landfill. Besides, high separation efficiency is one of the advantages of membrane separation method, but high maintenance cost and low economic feasibility are its disadvantages [16].

Among these methods, solid–phase extraction (SPE) plays an important role in sample pretreatment as it is characterized by its low consumption of solvents, high reproducibility, high preconcentration efficiencies, reduction of processing times, and low cost [17,18]. Moreover, it does not require devices of phase separation as in liquid–liquid extraction (LLE), DLLME and liquid-phase microextraction (LPME) methods [7,19–21]. There are different adsorbents as solid phase such as chitosan as adsorbent for removal of some organic dyes [22] and coal fly ash and modified montmorillonite clay with [23] zinc oxide (ZnO) nanoparticles have been investigated [24–28].

Agricultural by-products are an effective and economical alternative of adsorbents materials because of their chemical composition with abundant reactive groups since the hydroxyl groups are present in hemicellulose, cellulose and lignin which found in agricultural by-products have an affinity and reactivity towards heavy metals such as truffle peels that used for separation of Cr(VI) from aqueous solutions and organic pollutants such as natural pomegranate peels which used for separation of Rhodamine B dye from aqueous media [29–32].

Garlic peel (GP) is one of the agricultural wastes that can be obtained in most parts of the world. It has been used as biomass to remove organic and inorganic pollutants from the environment [33]. GP is a natural bio-fiber consisting of cellulose, hemicellulose and pectic components [34]. There are many functional groups present in these components such as hydroxyl, carboxyl and amino groups that assist in bond formation with many metals' ions [35].

Therefore, the objective of this study is exploring the ability and efficiency of modified garlic peels by nitric acid in order to remove Cr(VI) from aqueous media. Characterization of HNO_3 modified garlic peel (HNO_3-GP) as sorbent, studying the effect of optimum conditions such as pH of the medium, the dose of sorbent, initial Cr(VI) concentration, temperature and contact time on sorption process were studied. Furthermore, different kinetic models, various adsorption isotherms, thermodynamic parameters of the uptake Cr(VI) using the developed solid extractor were also studied. Finally, the validation of this methodology was supported by its application in real environmental water samples for the extraction of Cr(VI).

2. Experimental set-up

2.1. Reagents and materials

All chemicals used in this study were purchased from BDH Chemicals (Poole, England). Throughout the experiments, all glassware was cleaned using deionized water, followed by drying. Natural garlic peels were bought from a local market of Jeddah City which is located in the west region of Kingdom of Saudi Arabia. A standard stock solution (1,000 ppm) of $K_2Cr_2O_7$ was prepared by dissolving an accurate weight of the compound in 1,000 mL deionized distilled water. Solutions at different concentrations (5–30 ppm) were prepared by adding the appropriate amount of stock solution of Cr(VI). 1 M of HCl and 1 M of NaOH were used to adjust pH of the solution. Also, 1 M of HNO_3 was used to treated garlic peels.

2.2. Apparatus

In order to record the spectra and the absorbance measurements of Cr(VI) were made by UV-Vis Double Beam Spectrophotometer (GENESYS 10S Model, Thermo Scientific, New York) (200–700 nm) using a couple of quartz cuvette with 1 cm optical path length. A digital pH meter (Thermo Fisher Scientific Orine Model 720 pH meter) (Milford, MA, USA) was used for pH measurements of solutions. A shaker incubator (SI-100 model, HUMAN Lab, Korea) with a rate in the range of 10–300 rpm was used to shake and mix the solutions of Cr(VI) with HNO_3-GP in the conical flasks.

2.3. Recommended procedures

2.3.1. Preparation of HNO_3 modified garlic peel

Garlic was collected from a local market of Jeddah City, Kingdom of Saudi Arabia. Firstly, it was peeled and then washed with tap water for several times followed by washing with deionized distilled water to remove dust and other impurities. After that, GP was soaked in 500 mL of 1 M HNO_3 and kept for 4 h at laboratory temperature. Then, GP was washed with deionized distilled water for several times. Finally, HNO_3 modified garlic peel (HNO_3-GP) has been dried under sunlight for 5 d. Also, it was dried again in an oven at 70°C for 3 h. HNO_3-GP was turned into a fine powder by using an electric grinder (ELEKTA EFBG 1586 model) and it was sieved by a sieve with 0.85 mm. Then, it was stored in an airtight bottle.

2.3.2. Static experiments

The experiments were conducted to investigate the effects of some parameters including solution pH, initial concentration, adsorbent dose, contact time and temperature on the adsorption Cr(VI) by HNO_3-GP. In a series of conical flasks (50 mL), an accurate weight (0.5 ± 0.001 g) of HNO_3-GP was mixed with an aqueous solution (50 mL) containing Cr(VI) (5 ppm) at different pH (1–7). The mixture was shaken for 60 min on a mechanical shaker (SI-100 model, HUMAN Lab, Korea) with a rate in the range of 200 rpm was used for the equilibration experiments at 25°C. After adsorption, the mixture was filtered through filter paper and the adsorption efficiency was measured using UV-Vis Double Beam Spectrophotometer (GENESYS 10S Model, Thermo Scientific, New York) (200–700 nm). The concentration of Cr(VI) retained onto HNO_3-GP was then calculated from the difference between absorbance of Cr(VI) in the aqueous phase before and after extraction ($A_0 - A_f$) using HNO_3-GP, respectively. The extraction of percentage (%E), the amount

of Cr(VI) retained at equilibrium (q_e) and the distribution ratio (D) of Cr(VI) uptake by HNO_3-GP sorbent were determined by the following equations [36]:

$$\%E = \left(\frac{A_0 - A_f}{A_0} \right) \times 100 \quad (1)$$

$$q_e = \frac{\left(A_0 - A_f \right) V}{m} \quad (2)$$

$$D = \frac{\%E}{100 - \%E} \times \frac{V(\text{ml})}{w(g)} \quad (3)$$

where V and W represent the volume of the solutions (mL) and m is the amount of HNO_3-GP (g), respectively.

2.4. Sampling of real water

To examine the applicability of the suggested method for Cr(VI) removal, it was implemented on different environmental samples of water which were collected from Jeddah City, Kingdom of Saudi Arabia including bottle, tap and seawater. The tap water samples were attained from the chemistry laboratory at King Fahd Medical Research Centre and seawater samples were collected from the northern coastal area in Jeddah. All water samples (50 mL) were filtered through 0.45 μm cellulose membrane filter paper to remove any impurities before uses. Different concentrations (5–15 ppm) of Cr(VI) were then introduced to each type of water sample at pH ≈ 1 in presence of 0.5 g of HNO_3-GP and then was shaken separately for 20 min. All real water samples were analyzed using standard addition method under the batch conditions.

3. Results and discussion

Adsorbent materials used in solid phase extraction method play a major role in obtaining high extraction rates. Therefore, it is considered as one of the most important factors that has effect on the separation efficiency [17]. Therefore, the development of adsorbent materials to become more effective, economic and environmentally friendly has entice specific attention in this field. In addition, they are biodegradable and does not contain any unpleasant odor [30,37–39].

Lately, numerous studies have confirmed that chemical modification can promote selectivity or adsorption capacity of the biosorbents and decrease some organic materials released into solutions when functional groups are introduced or changed on the surface of agricultural by-products. Among of these biosorbents, GP has been used as a low-cost and an ideal biomass for pre concentration and removal of Cr(VI) in this study. GP is a natural bio-fiber consisting of cellulose, hemicellulose and pectic components [34]. There are many functional groups present in these components such as hydroxyl, carboxyl and amino groups that assist in bond formation with many metals' ions [35]. Ability of GP for sorption can be improved by optimizing several experimental factors. Thus, a detailed study on the characterization of natural and modified GP with HNO_3 in addition to its analytical application.

3.1. Characterization of GP adsorbent

Some techniques were utilized to make a complete characterization for GP before and after modification with HNO_3 such as scanning electron microscopy (SEM), energy-dispersive X-ray spectroscopy (EDX) and Fourier-transform infrared spectroscopy (FTIR).

The surface morphology of unmodified garlic peel and after modification with HNO_3 is depicted by SEM in Fig. 1. Fig. 1a and b show that unmodified GP with irregular and rough surface while Fig. 1d and c show that HNO_3-GP with a corroded net structure and large pore irregularly dispensed on the surface. Modification of garlic peel with HNO_3 could erode the surface of GP to generate more pores and increase the total pore volume thus increasing the surface area of GP, which assure that HNO_3-GP has a suitable surface morphology for binding heavy metal ions [40,41].

EDX Analysis was performed for natural garlic peel before and after modification with HNO_3 (Fig. 2a and b) which showed the proportions of main components for unmodified GP and modified GP with HNO_3, respectively. The results showed that the percentage of C decreased, while the percentage of O increased after modification by HNO_3. As the modification increases the number of acidic groups of oxygen which increases the surface area of GP. All these differences indicate a change in the chemical structure of the GP after modification by HNO_3 [33,42]. The existence of Ca element is due to the calcium component such as calcium pectate in the cell wall of GP. Ion-exchange between heavy metal ions in the solution and Ca^{2+} of GP was intended to be the adsorption process [40].

The difference in functional groups of unmodified garlic peel and after modification with HNO_3 is observed by spectra of FTIR in Fig. 3a and b. In both spectra, the broad and intense peaks from 3,500 to 3,000 cm^{-1} were observed, which indicate the presence of O–H or N–H stretching vibrations of amine due to inter- and intra-molecular hydrogen bonding of polymeric compounds (macromolecular associations), such as alcohols, phenols, and carboxylic acids, as in pectin, cellulose and lignin, thus, showing the presence of "free" hydroxyl groups on HNO_3-GP surface [40–42].

The peak observed at 2,920 cm^{-1} was attributed to C–H stretching vibrations of aliphatic acids. The peak from 1,700 to 1,850 cm^{-1} was characterized by C=O stretching vibrations of carboxylic acids. Besides the peak at 1,610 cm^{-1} was attributed to C=C or C=N while the peak at 1,055 cm^{-1} in both spectra attributed to C–O bending variation in –COOH. Aliphatic acid group vibration at 1,237 cm^{-1} may be assigned to deformation vibration of C=O and stretching formation of –OH of carboxylic acids and phenols [40]. The adsorptions in the range of 1,530 to 1,201 cm^{-1} in the spectra of HNO_3-GP were assigned to stretching of C=C bond in aromatic rings, which was not obviously observed in the spectra of GP. This might be related to the presence of aromatic rings [33].

In FTIR spectra of HNO_3-GP, the peak around 1,745 cm^{-1} (–COOH) was relatively stronger and the peak around 1,610 cm^{-1} ($–COO^-$) became relatively weaker compared with

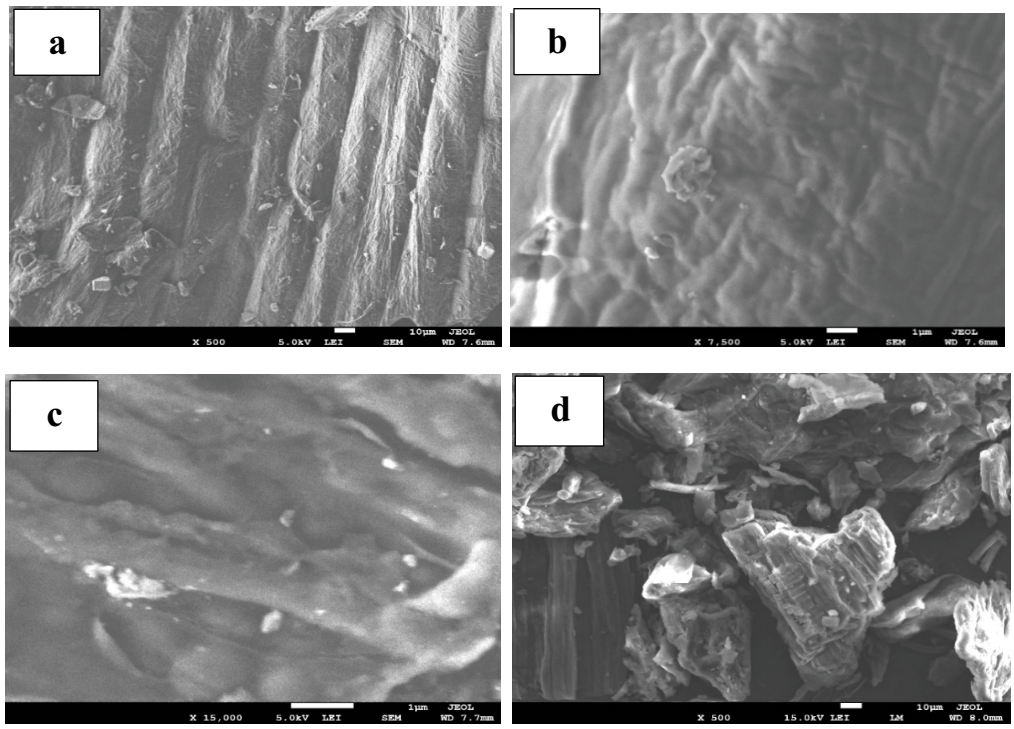

Fig. 1. Scanning electron micrographs of garlic peel (a,b) (500× and 7,500×) and HNO_3-GP (c,d) (15,000× and 500×).

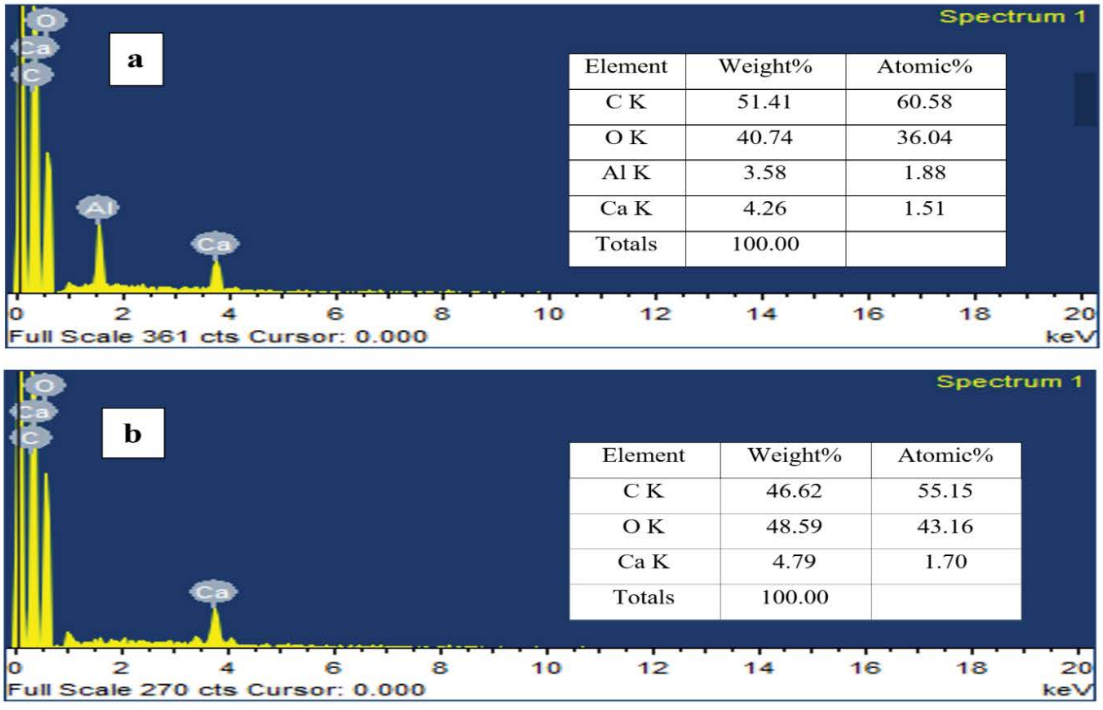

Fig. 2. Energy-dispersive X-ray spectroscopy of garlic peel (a) and HNO_3-GP (b).

the spectra of GP, which indicate that the modification by HNO_3 could cause oxidization of some unreactive groups into –COOH. This result confirmed the results of EDX where the percentage of oxygen increased in garlic peel after modification with HNO_3. Since the modification increases the surface acidic groups of oxygen which increases the surface area of GP.

Analysis of FTIR spectra indicated that the chemical modification led to different chemical properties, which causes an increase in the adsorption capacities [33,42].

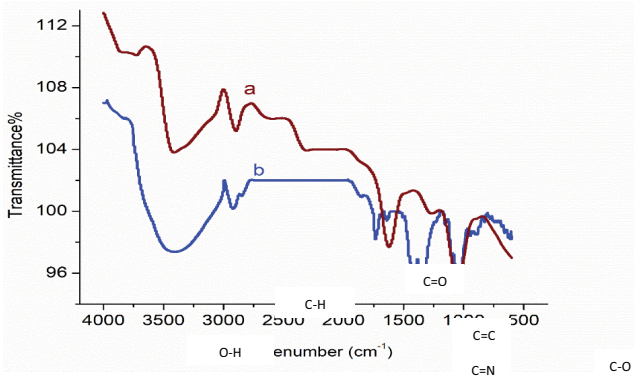

Fig. 3. Fourier-transform infrared spectra of garlic peel (a) and HNO_3-GP (b).

3.2. Effect of experimental variables on removal of Cr(VI) onto HNO_3-GP

The pH of the solution is one of the most important factors that controls the degree of ionization of the metal and the surface charge of the adsorbent [43]. The influence of pH (1–7) on the adsorption of Cr(VI) by HNO_3-GP in terms of the percentage of extraction is shown in Fig. 4.

The percentage of Cr(VI) extraction decreases by increasing the pH of solution from 1.0 to 7.0. It is important to pay attention that Cr(VI) extraction percentage achieved the maximum value (99.2%) at pH 1 thus, which was adopted in next experiments. Moreover, the existence of the functional groups such as phenolic –OH and carboxylic –COOH on HNO_3-GP surface bind electrostatically with negatively charged metal complex [$(CrO_3Cl)^-$]. Therefore, the decrease in the adsorption with increase in pH may be due to the decrease in electrostatic force of attraction between HNO_3-GP and Cr(VI) ions and the increased concentration of OH^- ions that complicates the adsorption process [3,33,44].

Extraction percentage (%E) of Cr(VI) was calculated by finding the difference between Cr(VI) absorbance before (A_0) and after (A_f) adsorption by HNO_3-GP, as mentioned before in Eq. (1):

$$\%E = \left(\frac{A_0 - A_f}{A_0}\right) \times 100 \quad (1)$$

Contact time is considered an effective factor to determine the probable order as well as time required to reach equilibrium for Cr(VI) adsorption onto HNO_3-GP. In this study, the effect of shaking time for 5 ppm of Cr(VI) from aqueous solutions at pH ≈ 1 by HNO_3-GP was investigated at a period of time ranging from 0.0 to 60.0 min.

The increasing of extraction percentage of Cr(VI) with increasing of shaking time resulted from the fast adsorption kinetics of HNO_3-GP toward Cr(VI) as shown in Fig. 5. Also, it is observed clearly in Fig. 5. that adsorbed Cr(VI) amount reached to 68% after 10 min, while the extraction percentage achieved the maximum value (100%) after 20 min. Thus, a shaking time of 20 min was adopted in next experiments.

The rate of adsorption of heavy metal ions was initially higher due to a ready availability of active sites on the adsorbent's surface. Further increase in contact time makes the adsorption rate less effective due to saturation of binding sites and accumulation of the heavy metal ions around the active site inhibited further adsorption [45].

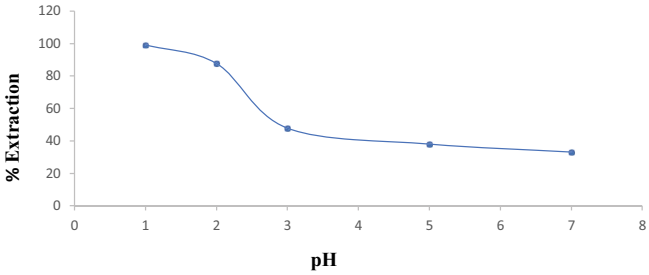

Fig. 4. Influence of pH on the adsorption of Cr(VI) onto HNO_3-GP at 25°C.

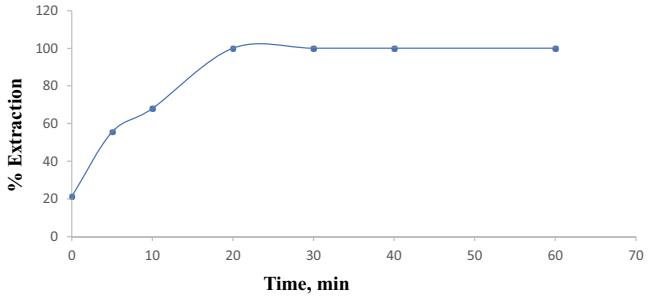

Fig. 5. Shaking time effect on the adsorption of Cr(VI) from aqueous solution onto HNO_3-GP after 1 h shaking time at 25°C.

The sorption percentage of a constant quantity of Cr(VI) (5 ppm) in aqueous medium (50 mL) was studied by varying HNO_3-GP dose (0.5–1.5 g) at pH ≈ 1 after 20 min shaking. The results are demonstrated in Fig. 6. Cr(VI) retention decreased on increasing HNO_3-GP dose from 0.5 to 1.5 g and reached maximum at a dose of 0.5 g where the percentage of removal was 99.2%. Thus, it no longer can increase with increasing dose of adsorbent. Due to potential aggregation and intraparticle interactions between HNO_3-GP molecules at the solid phase extractor, which resulted in a reduction in the total surface area of the HNO_3-GP and an increase in diffusional path length, this behavior is most likely explained by the decrease in the available adsorption site [41,46]. Therefore, 0.5 g was chosen for later removal studies.

3.3. Sorption isotherm of Cr(VI) retention by HNO_3-GP

Sorption isotherms were used to describe mechanism of the interaction of Cr(VI) ions on the sorbent surface. Depending on the nature of the sorption system, the equilibrium studies are useful to calculate the maximum sorption capacity of HNO_3-GP toward Cr(VI) ions and determine some important surface properties of the tested sorbent. The sorption characteristics of Cr(VI) ions wide range of equilibrium concentrations (5–30 ppm) from aqueous solution at pH ≈ 1 onto HNO_3-GP were studied at the optimized parameters.

Fig. 7 shows the plot of the amount of Cr(VI) retained (q_e) onto HNO_3-GP vs. the equilibrium concentration (C_e)

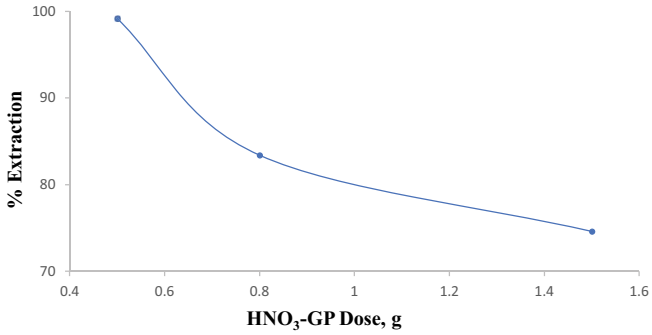

Fig. 6. Effect of different doses on the sorption percentage of Cr(VI) from the aqueous solutions on HNO_3-GP at pH ≈ 1 and 25°C.

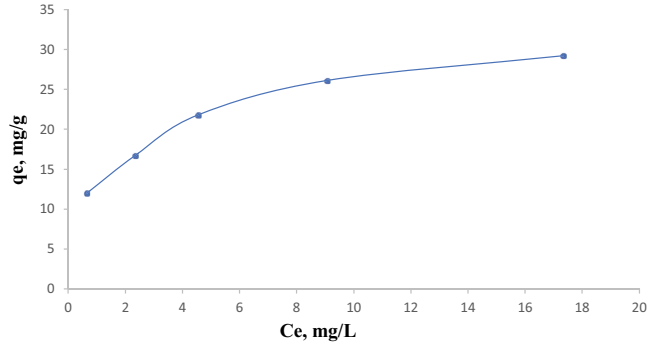

Fig. 7. Sorption isotherm of Cr(VI) uptake from the aqueous solution at optimum conditions onto HNO_3-GP at pH ≈ 1 and 25°C.

in the bulk aqueous solution. The plot shows a clear rise in Cr(VI) retained at low concentration followed by a convergent or slight rise at a concentration higher than 5 ppm. It is important to pay attention that Cr(VI) extraction percentage achieved the maximum value (86.96%) at 5 ppm of Cr(VI). This is indicating that at low equilibrium concentration of Cr(VI), the surface coverage of the adsorbent could be low and the available active sites of HNO_3-GP are not fully occupied by Cr(VI). The slight increase of the plot on increasing the analyte concentration due to an increase in the surface coverage and the restriction of the available active sites of HNO_3-GP [47,48].

The equilibrium data of this work were subjected to different adsorption isotherm models for example Langmuir, Freundlich and Dubinin–Radushkevich over a wide range of equilibrium concentration through linear regression in a condition of best fit.

3.3.1. Langmuir isotherm

The retention behavior of Cr(VI) from the aqueous solution onto HNO_3-GP was subjected to Langmuir model. This model assumes that the adsorption is a monolayer and a single layer of molecules on the adsorbent surface is absorbed. The solid surface of adsorbent is homogeneous and adsorption energy is uniform for all sites and the adsorption on the surface is localized which means that the atoms or

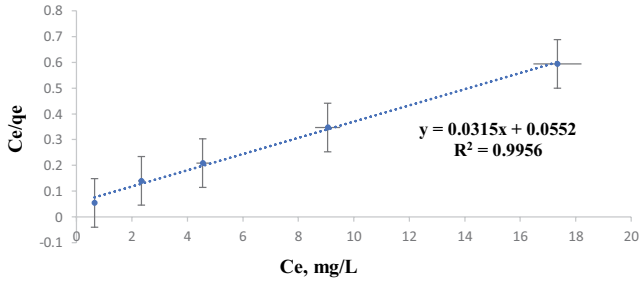

Fig. 8. Langmuir sorption isotherm of Cr(VI) uptake from the aqueous solution on HNO_3-GP surface at pH ≈ 1 and 25°C.

molecules are adsorbed at specific and localized sites [48–50]. The linear form of Langmuir model is expressed by the following equation [51]:

$$\frac{C_e}{q_e} = \frac{1}{K_L q_m} + \left(\frac{1}{q_m}\right) C_e \tag{4}$$

where C_e represents the equilibrium concentration of adsorbate (mg/L), q_e is the amount of adsorbate adsorbed per unit weight of adsorbent at equilibrium (mg/g), q_m donates the maximum adsorption capacity (mg/g) and K_L is the Langmuir constant (L/mg). The plot of C_e/q_e vs. C_e over the entire Cr(VI) concentration range as seen in Fig. 8.

Langmuir maximum adsorption capacity (q_m) and Langmuir constant (K_L) were calculated from the slope and intercept values and were found equal to 31.7 mg/g and 0.0552 L/mg, respectively. Moreover, the determination of correlation coefficient (R^2) for Langmuir model was 0.9956 that indicates the adsorption process is favorable and it is monolayer adsorption of Cr(VI) on the outer surface of HNO_3-GP [48].

The value of dimensionless constant (R_L) which is an equilibrium parameter referred to as separation factor is expressed as follows [51]:

$$R_L = \frac{1}{\left(1 + K_L C_0\right)} \tag{5}$$

where C_o is the initial concentration of adsorbate (mg/L). The dimensionless constant equilibrium parameter is mainly depending on the initial concentration at a given temperature. Table 1 clarifies R_L values at different initial concentration (C_o) of Cr(VI) at room temperature.

From the data obtained from Table 1, it was found that, at all initial concentrations, $0 < R_L < 1$ which confirms the favorable adsorption of Cr(VI) on the proposed sorbent.

3.3.2. Freundlich isotherm

Freundlich adsorption isotherm is a physical and empirical isotherm and another form of Langmuir that can be applied to multilayer adsorption. The stronger binding sites are occupied firstly, until adsorption energy is exponentially decreased upon the completion of adsorption process [48]. The linear form of the Freundlich model is expressed by the following equation [48]:

Table 1
R_L values at different initial concentration of Cr(VI)

C_o, mg/L	R_L
5	0.7837
10	0.6443
15	0.5470
20	0.4753
30	0.3765

$$\log q_e = \left(\frac{1}{n}\right)\log C_e + \log K_F \quad (6)$$

where K_F and n are Freundlich constants. K_F denotes the adsorption capacity (mg$^{1-(1/n)}$/L$^{1/n}$·g) and n indicates the adsorption intensity. The plot of logq_e against logC_e as shown in Fig. 9. Freundlich constants (1/n) and (K_F) were calculated from the slope and intercept values and were found equal 0.28 and 1.13 mg$^{1-(1/n)}$/L$^{1/n}$·g, respectively.

The value of (1/n) gets closer to 0, indicates that the surface of HNO_3-GP was more heterogeneous and the obtained value of the correlation coefficient (R^2 = 0.9889) which is close to value of (R^2 = 0.9956) in Langmuir model, indicating that the Freundlich model is applicable to describe the adsorption of Cr(VI) ions onto HNO_3-GP.

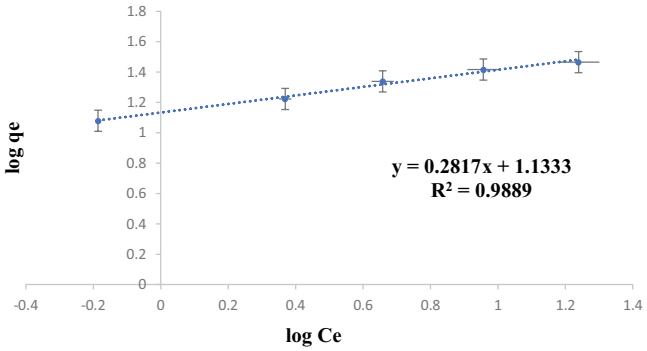

Fig. 9. Freundlich sorption isotherm of Cr(VI) uptake from the aqueous solution on HNO_3-GP surface at pH ≈ 1 and 25°C.

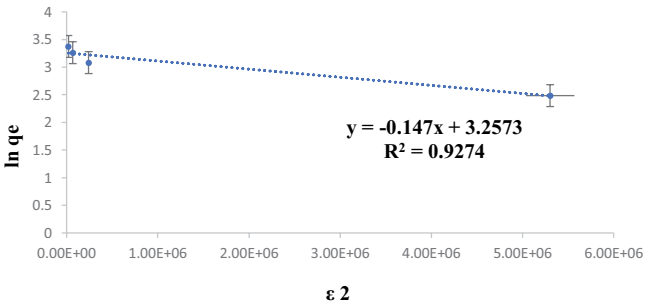

Fig. 10. Dubinin–Radushkevich sorption isotherm of Cr(VI) uptake from the aqueous solution on HNO_3-GP surface at pH ≈ 1 and 25°C.

3.3.3. Dubinin–Radushkevich isotherm

The Dubinin–Radushkevich adsorption isotherm model is applied to identify the characteristics of porosity, the mechanism of adsorption, and the free energy distribution onto a heterogeneous surface. This would precisely assign the nature of chemical or physical adsorption process of the retention step of Cr(VI) by the established solid adsorbent [48,52]. The linear form of this model is expressed as the following [48]:

$$\ln q_e = \ln q_{\max} - K_{DR}\varepsilon^2 \quad (7)$$

where K_{DR} is Dubinin–Radushkevich model constant indicates the adsorption energy (mol^2/kJ^2) and ε represents the Polanyi potential. The plot of lnq_e against ε^2 was linear (R^2 = 0.9274) as shown in Fig. 10. From Eq. (7) the slope equals to $-K_{DR}$ and the intercept equals to lnq_m. According to the plot in Fig. 10, the slope was found to be –0.147 so the value of Dubinin–Radushkevich constant (K_{DR}) was found to be 0.147 mol^2/kJ^2. The intercept value was found to be 3.2573, so the maximum adsorption capacity (q_m) equals to 25.9793 mg/g. Moreover, the value of mean free energy (E) for the biosorption process of Cr(VI) on the surface of HNO_3-GP can be calculated via the following equation [48]:

$$E = \frac{1}{\sqrt{2K_{DR}}} \quad (8)$$

The value of (E = 1.84 kJ/mol) achieved this condition E < 8 kJ/mol which confirms the adsorption process is physical process [48].

However, comparing the adsorption isotherm models applied, the Langmuir model gave the best fit, followed by the Freundlich isotherm and then the least fit was obtained with Dubinin–Radushkevich model. The parameters of these models of Cr(VI) uptake onto HNO_3-GP are summarized in Table 2.

3.4. Kinetics of Cr(VI) sorption on HNO_3-GP surface

Investigation of adsorption kinetics is important to explain the reaction mechanism. Therefore, Cr(VI) adsorption process onto HNO_3-GP was studied by various kinetic models for example Weber–Morris, pseudo-first-order, pseudo-second-order, Bhattacharya and Venkobachar, Elovich and finally Reichenberg model.

3.4.1. Intraparticle diffusion model

It is important to include diffusion-based kinetic modeling to clarify the role of diffusion processes, like film and intraparticle diffusion [53]. The data of this study were subjected to intraparticle diffusion rate model expressed by the Weber–Morris equation as the following [53]:

$$q_t = k_i t^{1/2} + C \quad (9)$$

where q_t is the amount of adsorbate adsorbed (mg/g), k_i is the rate of intraparticle diffusion (mg/g·min$^{1/2}$), t denotes the contact time (min) and C is a constant linked to the thickness of the boundary layer (mg/g).

Table 2
Calculated isotherm parameters for the adsorption of Cr(VI) onto HNO_3-GP

	Sorption isotherms models	HNO_3-GP
Langmuir	q_m (mg/g)	31.7
	K_L (L/mg)	0.0552
	R_L	0.784
	R^2	0.9956
Freundlich	$1/n$	0.28
	K_F (mg$^{1-(1/n)}$/L$^{1/n}$·g)	1.13
	R^2	0.9889
Dubinin–Radushkevich	q_m (mg/g)	25.9793
	K_{DR} (mol^2/kJ^2)	0.147
	E (kJ/mol)	1.84
	R^2	0.9274

The plot of q_t vs. time is displayed in Fig. 11. As shown, the plot was divided into two parts with two distinct slopes; the first one was linear with a high correlation value (R^2 = 0.9777) and the second stage was linear with a lower value (R^2 = 0.8151).

The adsorption sorption process of Cr(VI) by HNO_3-GP was very fast in the early stage and deviated by increasing the shaking time. The linear plot does not pass through the origin indicating that intraparticle diffusion is not the only the rate-controlling step. The diffusion rate was high firstly and then decreased by increase shaking period revealing that the rate of the retention step is film diffusion at the early stage of extraction. In the second stage, the diffusion remains fairly constant where the pores volume of HNO_3-GP were consumed.

Fig. 11 shows the values of k_i computed from the two distinct slopes in the initial and second stages of Weber–Morris plots for HNO_3-GP were found 4.0448 mg/g·min$^{1/2}$ and the second value was 0.3119 mg/g·min$^{1/2}$. This change in the slope is most likely due to the existence of different pore size.

The values of k_i indicated that intraparticle diffusion step can be considered as the rate controlling step, thus, the uptake of tested Cr(VI) onto the employed sorbent is most likely involved following three steps:

- Bulk transport of Cr(VI) in solution.
- Film transfer involving diffusion of Cr(VI) within the pore volume of the HNO_3-GP and/ or along the wall surface to the active sorption sites of the adsorbent.
- Finally, formation of the complex ion associate [48,53,54].

3.4.2. Pseudo-first-order model

The experimental data were also subjected to pseudo-first-order model. The linear form is given as [55]:

$$\log\left(q_e - q_t\right) = \log q_e - \frac{k_1}{2.303}t \tag{10}$$

where k_1 is the rate constant of pseudo-first-order (min^{-1}). The plot of log($q_e - q_t$) against time (t) as shown in Fig. 12.

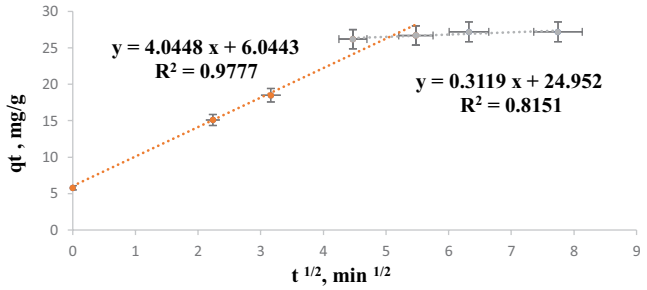

Fig. 11. Weber–Morris plot of Cr(VI) uptake from the aqueous solution onto HNO_3-GP at pH ≈ 1 and 25°C.

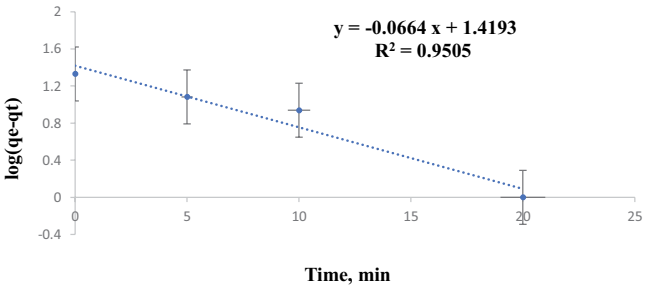

Fig. 12. Pseudo-first-order plot of Cr(VI) uptake from the aqueous solution onto HNO_3-GP at pH ≈ 1 and 25°C.

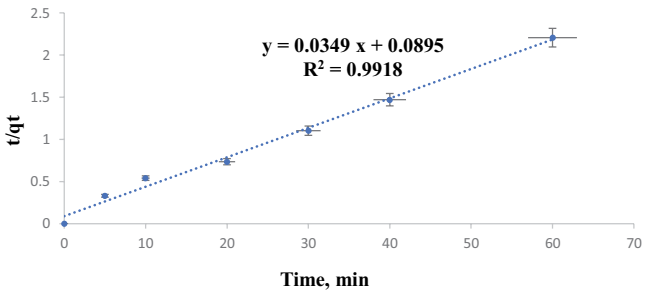

Fig. 13. Pseudo-second-order plot of Cr(VI) uptake from the aqueous solution onto HNO_3-GP at pH ≈ 1 and 25°C.

The value of correlation coefficient (R^2 = 0.9505). The slope is (–k/2.303) and the intercept is log(q_e). In addition, the calculated value k_1 and q_e were found to be 0.153 min^{-1} and 26.26 mg/g, respectively.

3.4.3. Pseudo-second-order model

Pseudo-second-order model assumed that two active adsorption sites were adsorbing one Cr(VI) ion on the adsorbent [54]. The linear form is given as the following [56]:

$$\frac{t}{q_t} = \frac{1}{h} + \frac{t}{q_e} \tag{11}$$

where $h = k_2 q_e^2$ that can be regarded as the initial rate of adsorption (mg/g·min) where k_2 is the rate constant of pseudo-second-order (g/mg·min). The plot of t/q_t vs. time (t) as shown in Fig. 13. The value of correlation coefficient (R^2 = 0.9918).

In addition, the calculated value of k_2 and h were found equal 0.0132 g/mg·min and 178.57 mg/g·min, respectively.

The straight line with excellent R^2 value obtained from the plot (Fig. 13) confirmed the fitness of pseudo-second-order model for the description of Cr(VI) removal using HNO_3-GP from aqueous solutions.

Good agreement between the values of the experimental value q_e (116.25 mg/g) and that is calculated value (117.6 mg/g) for pseudo-second-order kinetic model; these findings confirm the suitability of the pseudo-second-order equation for the description of Cr(VI) biosorption by the developed sorbent from aqueous solutions.

3.4.4. Bhattacharya and Venkobachar model

This model based on concentration of solution to study the mechanism of adsorption and characteristic constants of adsorption [57]. The linear form of this model is expressed as the following equation [57]:

$$\log\left[1-U(T)\right]=-\left(\frac{k_B}{2.303}\right)t \tag{12}$$

where $U(T)$ is the fractional attainment of equilibrium and k_B is constant of Bhattacharya and Venkobachar (min^{-1}). The value of k_B can be obtained from the slope of the linear plot of log[1–(U)T] against t which was 0.090 min^{-1}. Moreover, the correlation coefficient (R^2) was found to be 0.9768 as shown in Fig. 14.

3.4.5. Elovich model

This model has been used for the chemisorption process [58]. The linear form is given as the following [48]:

$$q_t=\left(\frac{1}{\beta}\right)\ln(\alpha\beta)+\left(\frac{1}{\beta}\right)\ln(t) \tag{13}$$

where α is the initial adsorption rate constant which give information about the high affinity (mg/g·min) and β is an adsorption constant linked to the extent of surface coverage (mg/g). The plot of q_t vs. ln$t$ will be linear (R^2 = 0.9703) and Elovich coefficients α and β can be determined from the slope and intercept of the plot, respectively. The slope value = 1/β while the intercept value = 1/β ln(αβ). As clarified in Fig. 15, the slope value equal 6.6159 so β = 0.1512 mg/g while the intercept value = 5.1195 so α = 14.34 mg/g·min.

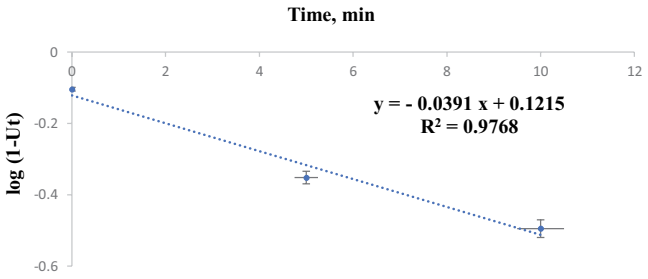

Fig. 14. Bhattacharya and Venkobachar model of Cr(VI) adsorption onto HNO_3-GP at pH ≈ 1 and 25°C.

The high α value gives strong indication about higher removal of Cr(VI) because of the higher surface area of HNO_3-GP that possessed strong adsorption active sites resulting in strong chemical binding with Cr(VI) ions. Also, the high correlation coefficient (R^2 = 0.9703) assures the applicability of Elovich model [59].

3.4.6. Reichenberg model

This model fully used broadly to describe the diffused films inside pores and represented as the following equations [60]:

$$F(t)=\left(1-\frac{6}{\pi^2}\right)e^{-Bt} \tag{14}$$

$$B_t=-0.4977-\ln\left(1-F(t)\right) \tag{15}$$

where B_t is the Reichenberg constant and F is a mathematical function, $F(t)$ = q_t/q_e is the ratio of amount of adsorbate adsorbed after time t to that at equilibrium time.

If the plot of B_t and t gave linear relation with higher correlation coefficient, this confirms the biosorption was due to film diffusion inside the internal pores of HNO_3-GP. As clarified in Fig. 16, a direct relation between B_t and time with higher R^2 therefore, that intraparticle diffusion is the rate controlling step with a small fraction of the sorption that occurs through film diffusion because the straight line does not pass through the origin [61].

A comparison between the values of R^2 for the data subjected to Weber–Morris, pseudo-first-order, pseudo-second-order, Bhattacharya and Venkobachar, Elovich and Reichenberg models revealed that pseudo-second-order model is reliable and more accurate than other models. Thus,

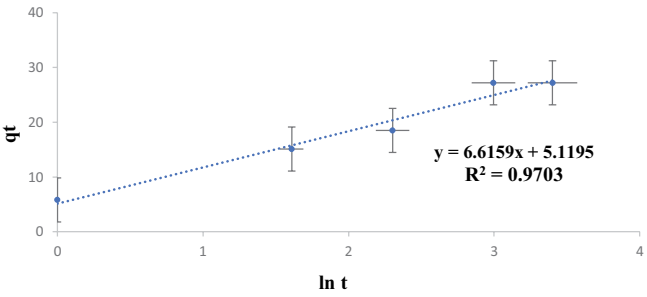

Fig. 15. Elovich plot of Cr(VI) adsorption onto HNO_3-GP at pH ≈ 1 and 25°C.

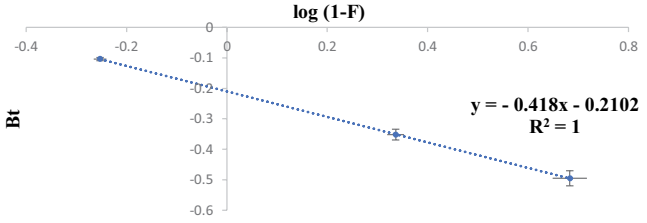

Fig. 16. Reichenberg plot of Cr(VI) adsorption onto HNO_3-GP at pH ≈ 1 and 25°C.

it can be concluded that the uptake of Cr(VI) by HNO_3-GP is most likely proceeds according to the second-order rate equation. The values of the adsorption of Cr(VI) onto HNO_3-GP for kinetic processes are summarized in Table 3.

3.5. Thermodynamic behavior of Cr(VI) retention onto HNO_3-GP

The sorption behavior of Cr(VI) by HNO_3-GP was critically studied over wide range of temperature (298–328 K) to determine the nature of Cr(VI) retention onto HNO_3-GP at the settled conditions. The thermodynamic parameters ($\Delta H°$, $\Delta S°$ and $\Delta G°$) can be expressed as the following equations [62]:

$$\Delta G° = \Delta H° - T\Delta S° \tag{16}$$

$$\ln K_c = \frac{-\Delta H}{RT} + \frac{\Delta S}{R} \tag{17}$$

where $\Delta G°$, $\Delta H°$, $\Delta S°$, R and T are the change of free energy (kJ/mol), the enthalpy change (kJ/mol), the entropy change (J/mol·K), the gas constant (8.314 J/mol·K) and temperature in Kelvin (K). K_c is the equilibrium constant for adsorption process of Cr(VI) from aqueous solution and its value can be calculated for adsorption of Cr(VI) employing the equation [62]:

$$K_c = \frac{\%E}{100 - \%E} \tag{18}$$

The plot of lnK_c vs. 1,000/T (K^{-1}) was linear over the entire temperature range from 298 to 328 K with good correlation coefficient (R^2 = 0.9993) as seen in Fig. 17.

From the displayed plot in Fig. 17, the enthalpy changes $\Delta H°$ was found to be 118.292 J/mol since the slope was equal to –14.228. Also, the entropy change $\Delta S°$ was found to be 394.39 J/mol·K since the intercept was equal to 47.437. Hence according to Gibb's Eq. (16), the change of free energy $\Delta G°$ was found to be –117.41 kJ/mol.

Table 3
Parameters of kinetic models for the adsorption of Cr(VI) onto HNO_3-GP

	Kinetic models	HNO_3-GP
Weber–Morris	k_i (mg/g·min$^{1/2}$)	4.0448 and 0.3119
	R^2	0.9777 and 0.8151
Pseudo-first-order	q_e (mg/g)	26.26
	k_1 (min^{-1})	0.153
	R^2	0.9505
Pseudo-second-order	q_e (mg/g)	117.6
	k_2 (g/mg·min)	0.0132
	R^2	0.9918
Bhattacharya and Venkobachar	k_B (min^{-1})	0.090
	R^2	0.9768
Elovich	α (mg/g·min)	14.34
	β (mg/g)	0.1512
	R^2	0.9703
Reichenberg	R^2	1

The negative value of $\Delta G°$ indicates that the adsorption of Cr(VI) onto HNO_3-GP is spontaneous while the positive value of $\Delta H°$ reflects the endothermic sorption process. In addition, the positive value of $\Delta S°$ reflects the affinity of HNO_3-GP for Cr(VI) and increases the randomness at the solid–solution interface with some structural changes in both adsorbate and adsorbent [55].

The enthalpy change $\Delta H°$ can be also calculated in terms of distribution ratio (D) from the slope of Van't Hoff plot according to the following equation [62]:

$$\log D = \frac{-\Delta H}{2.303RT} + C \tag{19}$$

The plot of log$D$ vs. 1,000/T shown in Fig. 18 was linear with good correlation coefficient (R^2 = 0.9993). $\Delta H°$ value for the sorption of Cr(VI) is equal to 118.32 J/mol. Thus, $\Delta H°$ agrees with the experimental value (118.292 J/mol) that was achieved from Eq. (17) and that confirms adsorption of Cr(VI) on surface of HNO_3-GP was endothermic sorption process. Also, the entropy change $\Delta S°$ was found to be 432.76 J/mol·K since the intercept was equal to 22.602. Hence according to Gibb's equation (16), the change of free energy $\Delta G°$ was found to be –128.88 kJ/mol.

The analytical aspects of the created approach were also successfully compared with a number of the reported methods [46,63–67]. The results are shown in Table 4. Moreover, features of heavy metals adsorption onto garlic peel as adsorbent were also effectively compared with several of the published papers as indicated in Table 5. The findings demonstrated that the suggested adsorbent (HNO_3-GP)

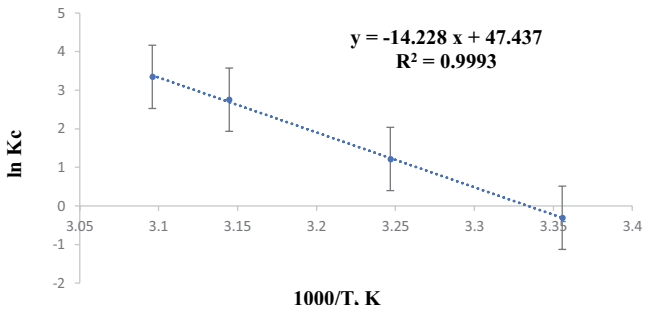

Fig. 17. Plot lnK_c vs. 1,000/T of Cr(VI) uptake from the aqueous solution onto HNO_3-GP at pH ≈ 1 and 25°C.

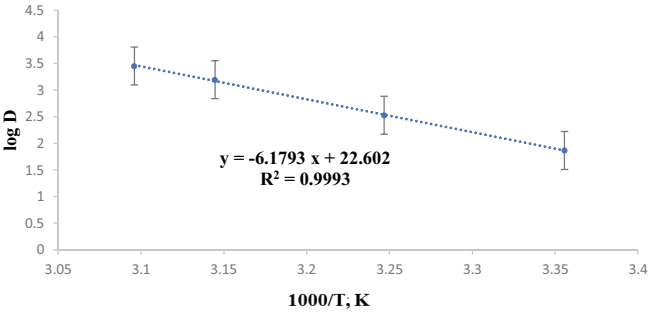

Fig. 18. Van't Hoff's plot of Cr(VI) uptake from the aqueous solution onto HNO_3-GP at pH ≈ 1 and 25°C.

Table 4
Analytical features of Cr(VI) adsorption onto various adsorbents

Adsorbent	Conc. Cr(VI) (ppm)	Contact time (min)	q_m (mg/g) (Langmuir)	References
Orange peels	10	50	1.9	[63]
Grafted banana peels	100	120	6.17	[64]
Soy hull biomass	50	120	7.286	[65]
Peanut shell	10	1440	8.31	[66]
Dragon fruit peel with fungal	25	60	11	[46]
Modified pomelo peel	5	2	21.55	[67]
Modified garlic peel	5	20	31.7	This study

Table 5
Analytical features of heavy metals adsorption onto garlic peel

Adsorbent	Metal	q_e (mg/g)	k_2 (g/mg·min)	Q_{max} (mg/g)	K_L (L/mg)	R^2	References
Native garlic peel	Pb^{+2}	58.04	0.01593	51.73	0.1303	0.990	[35]
		47.7	0.036	209	0.1120	0.998	
	Cu^{+2}	20.7	0.067	37.0	0.1290	0.996	[40]
	Ni^{+2}	17.2	0.235	32.0	0.5640	0.987	
NaOH mercerized garlic peel	Pb^{+2}	105.82	0.002619	109.05	0.2320	0.990	[35]
HNO_3 modified garlic peel	Cr+6	117.6	0.0132	31.7	0.0552	0.996	This work

Table 6
Analytical results of recovery percentage of Cr(VI) at different concentrations in real water samples

Sample	Cr(VI), μg·mL^{-1}		Recovery (%)
	Added	Found	
Bottle water	5	4.868 ± 0.132	97.37 ± 2.63
	10	9.886 ± 0.114	98.86 ± 1.14
	15	14.46 ± 0.54	96.43 ± 3.57
Tap water	5	4.6 ± 0.40	92.00 ± 7.50
	10	9.013 ± 0.987	90.13 ± 8.50
	15	12.59 ± 2.41	83.94 ± 8.90
Seawater	5	4.843 ± 0.157	96.85 ± 3.15
	10	9.962 ± 0.04	99.62 ± 0.38
	15	13.79 ± 1.21	91.95 ± 8.05

Average (n = 2) ± relative standard deviation.

offers a very efficient and affordable adsorbent in virtually completely removing heavy metals from the aqueous solution.

3.6. Applications of real samples

The applicability of the proposed adsorbent for Cr(VI) removal was examined by applying it, under batch conditions, on different environmental water samples that were collected from Jeddah City, Kingdom of Saudi Arabia including bottle, tap and seawater. Table 6. summarizes the results and shows good extraction percentages of Cr(VI) by using HNO_3-GP.

As shown in Table 6, the recovery percentage of Cr(VI) ranged from 83.94% to 99.62%. Therefore, the suggested method validated the suitability of HNO_3-GP to detect and remove Cr(VI) from real water samples.

4. Conclusion and future perspectives

The removal of Cr(VI) by HNO_3-GP was very fast. The results were confirmed that the best applicable isotherm model was Langmuir (R^2 = 0.9956) with excellent adsorption capacity of Cr(VI) (31.7 mg/g) that was achieved at optimum conditions. The results also indicated that the best appropriate kinetic model was pseudo-second-order. The adsorption of Cr(VI) from the aqueous solution on the proposed surface is an endothermic process depending on the positive value of enthalpy and spontaneous process based on the negative value of $\Delta G°$. On the other hand, the sign of entropy change was a positive value confirming that adsorption process was performed with high randomness on the surface of HNO_3-GP. Overall, the results were reliable, achievable and appropriate. Therefore, the proposed adsorbent can be successfully used for a selective separation of other heavy metals from the real water samples.

Conflict of interest

Authors disclose any potential conflict of interest including financial, personal or other relationships with other people or organizations within the time of beginning the submitted work that could inappropriately influence, or be perceived to influence their work.

References

[1] L. Joseph, B.-M. Jun, J.R.V. Flora, C.M. Park, Y. Yoon, Removal of heavy metals from water sources in the developing world using low-cost materials: a review, Chemosphere, 229 (2019) 142–159.

[2] S. Sadeghi, F.A. Rad, A.Z. Moghaddam, A highly selective sorbent for removal of Cr(VI) from aqueous solutions based on Fe_3O_4/poly(methyl methacrylate) grafted Tragacanth gum nanocomposite: optimization by experimental design, Mater. Sci. Eng., C, 45 (2014) 136–145.
[3] Ş. Parlayıcı, E. Pehlivan, Natural biosorbents (garlic stem and horse chesnut shell) for removal of chromium(VI) from aqueous solutions, Environ. Monit. Assess., 187 (2015) 763, doi: 10.1007/s10661-015-4984-6.
[4] L.L. Wang, J.Q. Wang, Z.X. Zheng, P. Xiao, Cloud point extraction combined with high-performance liquid chromatography for speciation of chromium(III) and chromium(VI) in environmental sediment samples, J. Hazard. Mater., 177 (2010) 114–118.
[5] A. Zhitkovich, Chromium in drinking water: sources, metabolism, and cancer risks, Chem. Res. Toxicol., 24 (2011) 1617–1629.
[6] M.B. Arain, I. Ali, E. Yilmaz, M. Soylak, Nanomaterial's based chromium speciation in environmental samples: a review, TrAC, Trends Anal. Chem., 103 (2018) 44–55.
[7] M. Pourmohammad, M. Faraji, S. Jafarinejad, Extraction of chromium(VI) in water samples by dispersive liquid–liquid microextraction based on deep eutectic solvent and determination by UV–Vis spectrophotometry, Int. J. Environ. Anal. Chem., 100 (2020) 1146–1159.
[8] E. Yilmaz, M. Soylak, Ultrasound assisted-deep eutectic solvent based on emulsification liquid phase microextraction combined with microsample injection flame atomic absorption spectrometry for valence speciation of chromium(III/VI) in environmental samples, Talanta, 160 (2016) 680–685.
[9] S. Kapitány, E. Sóki, J. Posta, Á. Béni, Separation/preconcentration of Cr(VI) with a modified single-drop microextraction device and determination by GFAAS, Acta Chim. Slov., 64 (2017) 248–255.
[10] Y.Y. Li, T.T. Zhang, Z. Ning, J.H. Chen, Characteristics and applications of sewage sludge biochar modified by ferrous sulfate for remediating Cr(VI)-contaminated soils, Adv. Civ. Eng., 2020 (2020) 1–11.
[11] M.S. Gaikwad, C. Balomajumder, Simultaneous rejection of chromium(VI) and fluoride [Cr(VI) and F] by nanofiltration: membranes characterizations and estimations of membrane transport parameters by CFSK model, J. Environ. Chem. Eng., 5 (2017) 45–53.
[12] U. Atikarnsakul, P. Varanusupakul, W. Alahmad, Isolation of chromium(VI) from aqueous solution by electromembrane extraction, Anal. Lett., 51 (2018) 983–997.
[13] S.K. Jawad, Joined liquid ion-exchange with cloud point extraction methods for separation and determination of Cr(VI), Mn(VII), J. Kufa Chem. Sci., 2 (2016) 195–201.
[14] A. Andrade-Eiroa, M. Canle, V. Leroy-Cancellieri, V. Cerdà, Solid-phase extraction of organic compounds: a critical review (Part I), TrAC, Trends Anal. Chem., 80 (2016) 641–654.
[15] A. Andrade-Eiroa, M. Canle, V. Leroy-Cancellieri, V. Cerdà, Solid-phase extraction of organic compounds: a critical review. Part II, TrAC, Trends Anal. Chem., 80 (2016) 655–667.
[16] F. Augusto, L.W. Hantao, N.G.S. Mogollón, S.C.G.N. Braga, New materials and trends in sorbents for solid-phase extraction, TrAC, Trends Anal. Chem., 43 (2013) 14–23.
[17] J. Płotka-Wasylka, N. Szczepańska, M. de la Guardia, J. Namieśnik, Modern trends in solid phase extraction: new sorbent media, TrAC, Trends Anal. Chem., 77 (2016) 23–43.
[18] S.A. Ahmed, M.A. Tantawy, E.M. Abdallah, M.I. Qassim, Characterization and application of kaolinite clay as solid phase extractor for removal of copper ions from environmental water samples, Int. J. Adv. Res. (IJAR), 3 (2015) 1–21.
[19] P. Gu, S. Zhang, X. Li, X. Wang, T. Wen, R. Jehan, A. Alsaedi, T. Hayat, X. Wang, Recent advances in layered double hydroxide-based nanomaterials for the removal of radionuclides from aqueous solution, Environ. Pollut., 240 (2018) 493–505.
[20] X. Liu, R. Ma, X. Wang, Y. Ma, Y. Yang, L. Zhuang, S. Zhang, R. Jehan, J. Chen, X. Wang, Graphene oxide-based materials for efficient removal of heavy metal ions from aqueous solution: a review, Environ. Pollut., 252 (2019) 62–73.
[21] M. Tian, L. Fang, X. Yan, W. Xiao, K.H. Row, Determination of heavy metal ions and organic pollutants in water samples using ionic liquids and ionic liquid-modified sorbents, J. Anal. Methods Chem., 2019 (2019) 1948965, doi: 10.1155/2019/1948965.
[22] Z. Saigl, O. Tifouti, B. Alkhanbashi, G. Alharbi, H. Algamdi, Chitosan as adsorbent for removal of some organic dyes: a review, Chem. Pap., 77 (2023) 2363–2405.
[23] E. Altıntıg, S. Balta, M. Balta, Z. Aydemır, Methylene blue removal with ZnO coated montmorillonite: thermodynamic, kinetic, isotherm and artificial intelligence studies, Int. J. Phytorem., 24 (2022) 867–880.
[24] H. Karaca, E. Altıntığ, D. Türker, M. Teker, An evaluation of coal fly ash as an adsorbent for the removal of methylene blue from aqueous solutions: kinetic and thermodynamic studies, 39 (2018) 1800–1807.
[25] P.S. Koujalagi, H.N. Revankar, R.M. Kulkarni, V.R. Gurjar, Sorption of chromium(VI) from electroplating rinse water by strong base anion exchanger: equilibrium and kinetic studies, J. Phys. Conf. Ser., 1913 (2021) 012076, doi: 10.1088/1742-6596/1913/1/012076.
[26] H. Sereshti, M. Vasheghani Farahani, M. Baghdadi, Trace determination of chromium(VI) in environmental water samples using innovative thermally reduced graphene (TRG) modified SiO_2 adsorbent for solid phase extraction and UV-vis spectrophotometry, Talanta, 146 (2016) 662–669.
[27] P.S. Koujalagi, S.V. Divekar, R.M. Kulkarni, R.K. Nagarale, Kinetics, thermodynamic, and adsorption studies on removal of chromium(VI) using Tulsion A-27(MP) resin, Desal. Water Treat., 51 (2013) 3273–3283.
[28] P.S. Koujalagi, S.V. Divekar, R.M. Kulkarni, E.M. Cuerda-Correa, Sorption of hexavalent chromium from water and water–organic solvents onto an ion exchanger Tulsion A-23(Gel), Desal. Water Treat., 57 (2016) 23965–23974.
[29] A. Bhatnagar, M. Sillanpää, A. Witek-Krowiak, Agricultural waste peels as versatile biomass for water purification – a review, Chem. Eng. J., 270 (2015) 244–271.
[30] P.D. Pathak, S.A. Mandavgane, B.D. Kulkarni, Fruit peel waste as a novel low-cost bio adsorbent, Rev. Chem. Eng., 31 (2015) 361–381.
[31] Z.M. Saigl, A.M. Ahmed, Separation of Rhodamine B dye from aqueous media using natural pomegranate peels, Indones. J. Chem., 21 (2021) 212–224.
[32] Z.M. Saigl, S.M. Al-Dafeeri, Selective separation of chromium(VI) from aqueous solutions by adsorption onto truffle peels as novel biomass, Int. J. Environ. Anal. Chem., 103 (2021) 928–946.
[33] Y. Zhao, W. Li, J. Liu, K. Huang, C. Wu, H. Shao, H. Chen, X. Liu, Modification of garlic peel by nitric acid and its application as a novel adsorbent for solid-phase extraction of quinolone antibiotics, Chem. Eng. J., 326 (2017) 745–755.
[34] P. Muthamilselvi, R. Karthikeyan, A. Kapoor, S. Prabhakar, Continuous fixed-bed studies for adsorptive remediation of phenol by garlic peel powder, Int. J. Ind. Chem., 9 (2018) 379–390.
[35] W. Liu, Y. Liu, Y. Tao, Y. Yu, H. Jiang, H. Lian, Comparative study of adsorption of Pb(II) on native garlic peel and mercerized garlic peel, Environ. Sci. Pollut. Res., 21 (2014) 2054–2063.
[36] M.S. El-Shahawi, H.A. Nassif, Retention and thermodynamic characteristics of mercury(II) complexes onto polyurethane foams, Anal. Chim. Acta, 481 (2003) 29–39.
[37] Y. Xiong, L. Wan, J. Xuan, Y. Wang, Z. Xing, W. Shan, Z. Lou, Selective recovery of Ag(I) coordination anion from simulate nickel electrolyte using corn stalk based adsorbent modified by ammonia–thiosemicarbazide, J. Hazard. Mater., 301 (2016) 277–285.
[38] M.S. Abdel-Raouf, A.R.M. Abdul-Raheim, Removal of heavy metals from industrial waste water by biomass-based materials: a review, J. Pollut. Eff. Control, 5 (2016) 1–13.
[39] D. Setyono, S. Valiyaveettil, Functionalized paper—a readily accessible adsorbent for removal of dissolved heavy metal salts and nanoparticles from water, J. Hazard. Mater., 302 (2016) 120–128.

[40] S. Liang, X. Guo, Q. Tian, Adsorption of Pb^{2+}, Cu^{2+} and Ni^{2+} from aqueous solutions by novel garlic peel adsorbent, Desal. Water Treat., 51 (2013) 7166–7171.
[41] P. Muthamilselvi, R. Karthikeyan, B.S.M. Kumar, Adsorption of phenol onto garlic peel: optimization, kinetics, isotherm, and thermodynamic studies, Desal. Water Treat., 57 (2016) 2089–2103.
[42] Y. Zhao, L. Zhu, W. Li, J. Liu, X. Liu, K. Huang, Insights into enhanced adsorptive removal of Rhodamine B by different chemically modified garlic peels: comparison, kinetics, isotherms, thermodynamics and mechanism, J. Mol. Liq., 293 (2019) 111516, doi: 10.1016/j.molliq.2019.111516.
[43] M. Siahkamari, A. Jamali, A. Sabzevari, A. Shakeri, Removal of lead(II) ions from aqueous solutions using biocompatible polymeric nano-adsorbents: a comparative study, Carbohydr. Polym., 157 (2017) 1180–1189.
[44] K. Mulani, S. Daniels, K. Rajdeo, S. Tambe, N. Chavan, Adsorption of chromium(VI) from aqueous solutions by coffee polyphenol-formaldehyde/acetaldehyde resins, J. Polym., 2013 (2013) 1–11.
[45] M. Hasanpour, M. Hatami, Application of three dimensional porous aerogels as adsorbent for removal of heavy metal ions from water/wastewater: a review study, Adv. Colloid Interface Sci., 284 (2020) 102247, doi: 10.1016/j.cis.2020.102247.
[46] A. Saravanan, P. Senthil Kumar, S. Varjani, S. Karishma, S. Jeevanantham, P.R. Yaashikaa, Effective removal of Cr(VI) ions from synthetic solution using mixed biomasses: kinetic, equilibrium and thermodynamic study, J. Water Process Eng. 40 (2021) 101905, doi: 10.1016/j.jwpe.2020.101905.
[47] U.O. Aigbe, O.A. Osibote, A review of hexavalent chromium removal from aqueous solutions by sorption technique using nanomaterials, J. Environ. Chem. Eng., 8 (2020) 104503, doi: 10.1016/j.jece.2020.104503.
[48] R. Saadi, Z. Saadi, R. Fazaeli, N.E. Fard, Monolayer and multilayer adsorption isotherm models for sorption from aqueous media, Korean J. Chem. Eng., 32 (2015) 787–799.
[49] S. Rangabhashiyam, N. Anu, M.S. Giri Nandagopal, N. Selvaraju, Relevance of isotherm models in biosorption of pollutants by agricultural byproducts, J. Environ. Chem. Eng., 2 (2014) 398–414.
[50] B. Nagy, C. Mânzatu, A. Măicăneanu, C. Indolean, L. Barbu-Tudoran, C. Majdik, Linear and nonlinear regression analysis for heavy metals removal using *Agaricus bisporus* macrofungus, Arabian J. Chem., 10 (2017) S3569–S3579.
[51] R.R. Karri, J.N. Sahu, N.S. Jayakumar, Optimal isotherm parameters for phenol adsorption from aqueous solutions onto coconut shell based activated carbon: error analysis of linear and non-linear methods, J. Taiwan Inst. Chem. Eng., 80 (2017) 472–487.
[52] J. Wang, X. Guo, Adsorption isotherm models: classification, physical meaning, application and solving method, Chemosphere, 258 (2020) 127279, doi: 10.1016/j.chemosphere.2020.127279.
[53] B. Obradovic, Guidelines for general adsorption kinetics modeling, Hem. Ind., 74 (2020) 65–70.
[54] H.K. Boparai, M. Joseph, D.M. O'Carroll, Kinetics and thermodynamics of cadmium ion removal by adsorption onto nano zerovalent iron particles, J. Hazard. Mater., 186 (2011) 458–465.
[55] Y.S. Kim, J.H. Kim, Isotherm, kinetic and thermodynamic studies on the adsorption of paclitaxel onto Sylopute, J. Chem. Thermodyn., 130 (2019) 104–113.
[56] M. Matouq, N. Jildeh, M. Qtaishat, M. Hindiyeh, M.Q. Al Syouf, The adsorption kinetics and modeling for heavy metals removal from wastewater by *Moringa* pods, J. Environ. Chem. Eng., 3 (2015) 775–784.
[57] P.A. Ekwumemgbo, J.A. Kagbu, A.J. Nok, K.I. Omoniyi, Kinetics of gamma globulin adsorption onto titanium, Rasayan J. Chem., 3 (2010) 221–231.
[58] J. Wang, X. Guo, Adsorption kinetic models: physical meanings, applications, and solving methods, J. Hazard. Mater., 390 (2020) 122156, doi: 10.1016/j.jhazmat.2020.122156.
[59] S. Khaoya, U. Pancharoen, 168-Ca209, 3 (2012) 98–103.
[60] J.O. Vinhal, M.R. Lage, J.W.M. Carneiro, C.F. Lima, R.J. Cassella, Modeling, kinetic, and equilibrium characterization of paraquat adsorption onto polyurethane foam using the ion-pairing technique, J. Environ. Manage., 156 (2015) 200–208.
[61] D. Reichenberg, Properties of ion-exchange resins in relation to their structure. III. Kinetics of exchange, J. Am. Chem. Soc., 75 (1953) 589–597.
[62] C.Y. Abasi, I.P. Ejidike, E.D. Dikio, Synthesis, characterisation of ternary layered double hydroxides (LDH) for sorption kinetics and thermodynamics of Cd^{2+}, Int. J. Environ. Stud., 76 (2019) 441–455.
[63] G. López-Téllez, C.E. Barrera-Díaz, P. Balderas-Hernández, G. Roa-Morales, B. Bilyeu, Removal of hexavalent chromium in aquatic solutions by iron nanoparticles embedded in orange peel pith, Chem. Eng. J., 173 (2011) 480–485.
[64] A. Ali, K. Saeed, F. Mabood, Removal of chromium(VI) from aqueous medium using chemically modified banana peels as efficient low-cost adsorbent, Alexandria Eng. J., 55 (2016) 2933–2942.
[65] P.S. Blanes, M.E. Bordoni, J.C. González, S.I. García, A.M. Atria, L.F. Sala, S.E. Bellú, Application of soy hull biomass in removal of Cr(VI) from contaminated waters. Kinetic, thermodynamic and continuous sorption studies, J. Environ. Chem. Eng., 4 (2016) 516–526.
[66] Z.A. AL-Othman, R. Ali, Mu. Naushad, Hexavalent chromium removal from aqueous medium by activated carbon prepared from peanut shell: adsorption kinetics, equilibrium and thermodynamic studies, Chem. Eng. J., 184 (2012) 238–247.
[67] Q. Wang, C. Zhou, Y.-j. Kuang, Z.-h. Jiang, M. Yang, Removal of hexavalent chromium in aquatic solutions by pomelo peel, Water Sci. Eng., 13 (2020) 65–73.